Proceedings of the Thirtieth (2020) International Ocean and Polar Engineering Conference **www.isope.org**
Shanghai, China, October 11-16, 2020

ISBN 978-1-880653-84-5; ISSN 1098-6189

Numerical Simulation of Bow Waves Generated by a Rectangular Plate

*Yiding Hu, Cheng Liu, Decheng Wan**

Computational Marine Hydrodynamics Lab (CMHL), State Key Laboratory of Ocean Engineering,
School of Naval Architecture, Ocean and Civil Engineering, Shanghai Jiao Tong University, Shanghai, China
*Corresponding author

ABSTRACT

The scope of this work is to present and discuss the results obtained from simulating the bow wave generated by a ship advancing in calm water. A rectangular flat plate is used instead of a ship owing to its remarkable simplicity. The simulations are performed based on the block-based adaptive mesh refinement to provide adequate higher resolution where needed. Immersed boundary method is adopted to simulate a moving rectangular flat immersed in fluid. Bow wave height and the distance between a ship stem and bow wave crest are main parameters we focus on. Some details of bow-wave are also shown in the present study.

KEY WORDS: ship bow waves; numerical simulation; a rectangular flat plate; adaptive mesh; immersed boundary method.

INTRODUCTION

The bow waves are frequently observed at the stem of a high-speed ship. The features of ship bow waves are very important for hydrodynamic design at the early stage. Owing to the limitation of numerical methods and calculation capacity, the main means to study ship bow wave are experiments and theoretical methods in the last few decades. Dong et al. (1997) investigated the origin of the bow wave, the structure of the bow wave and the point at which the bow wave separates from the ship by Particle Image Velocimetry (PIV) measurements and free-surface visualizations on a ship model. They discovered that the Fr=0.45 case showed boundary layer separation and the generation of vorticity near the crest of the bow wave. The vorticity generated at the peak of the bow wave was transferred downstream and produced a series of small-scale free surface depressions. Waniewski et al. (2001) investigated the dynamics and air entrainment processes of a ship bow wave by numerical simulations. The waves were generated by a deflecting plate in a free surface flow in water channel. They mainly focused on how the bow wave changed with the flow and geometric parameters. Ship bow waves were simulated with a method known as 2D+T by Shakeri et al. (2006) and wave profile measurements were presented for a range of equivalent full-scale ship speeds ranging from 16.5 to 27 knots. They also discovered that the maximum height of the bow wave and the rise of the contact line increase with increasing equivalent ship speed. Olivieri et al. (2007) conducted a photographic study and some measurements for Fr=0.35 to study wave breaking for the surface combatant. Authors noticed this case contained an energetic plunging breaking bow wave and a steep spilling breaking wave.

Numerous researchers have investigated many simple expressions for ship bow waves based on the mathematical analysis, the dimensional analysis and theoretical considerations. Ogilvie (1972) proposed a simple analytical expression that defines the height of a ship bow wave in terms of the ship speed, the waterline entrance angle and the ship drift by a complicated mathematical analysis. Waniewski et al. (2002) used a set of experimental measurements to modify Ogilvie's expression. Noblesse et al. (2006) used dimensional analysis and other fundamental theoretical considerations to yield a simple approximation which is in excellent agreement with experimental data. Noblesse et al. (2008) concluded two main types of ship bow waves: 'unsteady bow waves' and 'overturning bow waves' that are stable and steady (until the plunging waves hit the free surface). The two bow waves also are called 'spilling' and 'plunging' waves widely in the study of wave breaking. Delhommeau et al. (2009) analyzed the boundary between the overturning bow wave and unsteady bow wave and considered some complicated ship bows with rake and flare.

With the rapid development of computational fluid dynamics (CFD) technology, accurate simulation of the ship bow wave with the advantage of capturing more details becomes possible. Two-dimensional detailed wave breaking processes and velocity profiles were obtained for plunging wave breaking by Chen et al. (1999). The nonlinear wave breaking on the free surface are well simulated around an advancing two-dimensional rectangular cylinder by Kim and Lee (2001). It is confirmed that the numerical method is useful for the complex flow by the comparisons between the simulation results and the experiments. Wilson et al. (2007) used an unsteady single-phase level RANS method to study bow wave breaking around a ship in calm water. Small-scale features of 3D ship breaking waves were resolved with local over-set grid refinement. A global description of bow wave breaking and induced vortices and scars are provided which allow for a further understanding of such flows. Lubin and Glockner (2011) studied the fine structure

generated during the early stage of three-dimensional plunging wave breaking and the subsequent air entrainment. Two different methods are used to simulate the flow around the DDG 5415 by Dommermuth et al. (2004), "coupled level-set and volume-of-fluid (CLS)" method and "level-set (LS)" method. The ship wave results indicate that the two methods can simulate the complex flow around a ship. The breaking wave of DTMB 5415 in calm water was investigated using naoe-FOAM-SJTU solver by Wang and Wan (2018, 2020), Wang, Ren and Wan (2019), Wang, Zhao and Wan (2019).

The object of this paper is to simulate ship bow waves accurately and consider explicit relationships between main parameters of a ship bow wave and basic ship design parameters. The results of numerical simulation will be compared with measurements and observations for a rectangular flat towed in the towing tank of Ecole Centrale de Nantes and a simple expression proposed by Noblesse et al. (2006) to verify the accuracy of the simulation. The results of numerical simulation are used to solve the nondimensional number which is in the simple expression. The overturning and the unsteady bow wave are also considered here.

NUMERICAL METHODS

Governing Equation

The governing equations for the present computations are the following Navier-Stokes equation and the continuity equation of three-dimensional incompressible viscous flow. The expression can be written as

$$(\partial_t \rho U + \nabla \cdot (pUU)) = -\nabla p + \nabla \cdot (2\mu D) + pg + T_\sigma \quad (1)$$

$$\partial_t \rho + \nabla \cdot (\rho U) = 0 \quad (2)$$

where U= (u, v, w) the fluid velocity, ρ the fluid density, μ the dynamic viscosity. D represents the deformation tensor which is defined as $D_{i,j} = (\partial_i u_j + \partial_j u_i)/2$. $T_\sigma = \gamma k \delta_s n$, δ_s, indicating that the surface tension term which is concentrated on the interface, where γ, k, n are the surface tension coefficient, the interfacial curvature and the interface unit normal.

The VOF equation is expressed as

$$\frac{\partial \chi}{\partial t} + \nabla \cdot (\chi U) - \chi \nabla \cdot U = 0 \quad (3)$$

$$\chi(x,y) = \begin{cases} 1 & \text{liquid in cell} \\ 0 & \text{gas in cell} \end{cases}$$

where $\chi(x,y)$ is phase function, which represents the distribution of the free surface. When $\chi(x,y)$ is equal to 0, the gird is full of gas; when $\chi(x,y)$ is equal to 1, the grid is full of liquid; when $\chi(x,y)$ is between 0 and 1, the cell contains a free surface.

The density ρ and viscosity μ in Eqs. 1~2 are computed using the volume fraction in Eq. 3.

$$\rho = \chi \rho_l + (1-\chi)\rho_g \quad (4)$$

$$\mu = \chi \mu_l + (1-\chi)\mu_g \quad (5)$$

l and g represent the fluid and liquid phase respectively.

Immersed boundary method

An efficient immersed boundary method proposed by Liu and Hu (2014) is adopted to simulate a moving rectangular flat immersed in fluid. In immersed boundary method, a volume force term, which is determined by time and space discrete scheme, is introduced in Navier-Stokes equations to impose the boundary conditions. A MLS (moving least square) interpolation method based on level set function is proposed to reconstruct the velocity on the forcing points. The velocity at the forcing point is determined by the MLS interpolation using the points in supporting domain. By applying the efficient moving surface tracking strategy, the level set function based on MLS-IB method is found to be more flexible in dealing with the moving rigid body and achieve high-precision motion response prediction and analysis of complex flow characteristics around the body surface.

In the present study, the benefits are that the grid generation can be simplified for a moving rectangular flat and adaptive cartesian grids can be directly implemented.

Block-based adaptive mesh refinement

As we know, the simulation result will be more accurate if we adopt more fine grids. However, a large number of grids will affect computation efficiency seriously and more time will be wasted. In the simulation of a rectangular flat towed in fluid, the region of the free surface is that we care about. We can improve the local resolution while ensuring the calculation efficiency by using adaptive mesh refinement mesh. Block-based adaptive mesh refinement proposed by Liu and Hu (2018) is used to improve computational efficiency. The adaptive mesh refinement is performed by using blocks. All the blocks have identical logical structure, thus the same algorithms can be used in different block levels. Tree structure is adopted to manage data and conservative interpolation algorithm which is used for information transmission among blocks with different refinement level. By using mesh refinement method, dynamic load-balancing algorithm and data communication technique, the computational workload can be concentrated only in the necessary region, which greatly improves the large-scale parallel computational efficiency for typical problems.

SIMULATION SETUP

A series of numerical simulations of a rectangular flat plate towed in fluid were performed. The flat plate is 0.782m long and 0.5m high immersed at the draft D=0.2m or 0.3m as Fig. 1 (draft is 0.2m). The speeds of the flat plate are U=1.5, 1.75, 2, 2.25, 2.5 m/s and the draft Froude number varies from 0.8 to 1.8. The value of the incidence angle is α_E=10-20-30 deg and the values of flare angle are γ =0-10-15 deg.

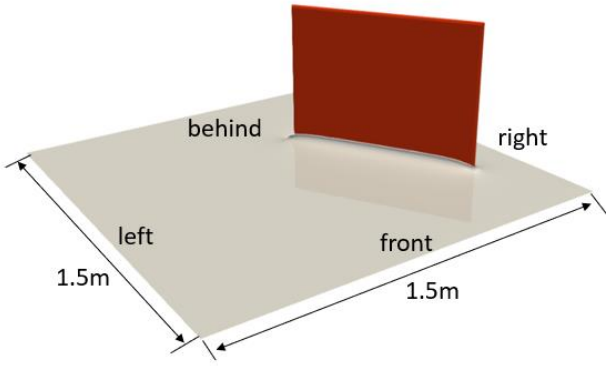

Fig. 1 The arrangement of numerical simulation with the incidence angle α_E=30°, the flare angle $\gamma = 0°$ and draft D=0.2m

Table 1. Ten cases with various incidence angle α_E, Flare angle γ, U and draft D.

Number	Incidence angle α_E(deg)	Flare angle γ(deg)	U(m/s)	F_D
Case 1	10	10	1.75	1.2495
Case 2	10	10	2.5	1.7848
Case 3	20	0	2.5	1.7848
Case 4	20	15	1.75	1.2495
Case 5	20	15	2.5	1.7848
Case 6	20	15	2.25	1.6063
Case 7	30	0	1.25	0.8924
Case 8	30	0	2.0	1.4278
Case 9	30	10	1.75	1.2495
Case 10	30	15	2.25	1.6063

The arrangement of the numerical simulation of a rectangular flat plate towed in fluid which is corresponding to case8 with the incidence angle α_E=30°, the flare angle $\gamma = 0°$ and draft D=0.2m is depicted in Fig. 1. Ten different cases are simulated in the present study which are concluded in Table 1.

Computational domain and boundary Condition

The arrangement of computational domain is depicted in Fig. 1. The 3D numerical domains are discretized into about 4 million non-regular Cartesian cells. Inflow and outflow boundary conditions were imposed in the wave propagation direction. The slip boundary conditions were applied to the left and right sides. The bottom is wall condition and the top is atmosphere condition.

Main parameters of the ship bow wave

In this paper, we mainly focus on the following parameters. Z_b, the height of the bow wave, is the distance between the crest of ship bow wave and the mean free-surface plane. X_b, the location of the crest of ship bow wave, is the distance between the ship stem and the crest of ship bow wave. The two parameters and draft D were expressed in Fig. 2. The half waterline entrance angle is also shown in Fig. 2.

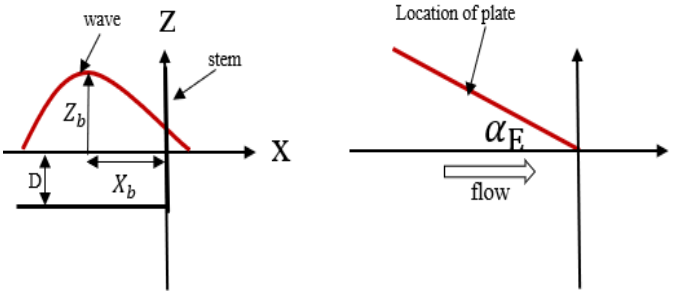

Fig. 2 Sketch that defines main parameters Z_b, X_b, D and α_E. Z_b and X_b represent the height and location of the ship bow wave. D and α_E are draft and the half waterline entrance angle.

RESULT AND DISSCUSION

Overturning and unsteady bow wave

Two types of ship bow wave can be observed: overturning bow waves and unsteady bow waves. On the left and right sides of Fig. 3 which is from Noblesse at el. (2008), overturning bow waves and unsteady bow waves are shown. A simple criterion that defines steady bow wave or unsteady bow wave is proposed by Noblesse et al. (2008). When the waterline entrance angle is smaller than approximately 25 deg, the steady overturning wave is generated by ship at any Froude number owing to a sufficiently waterline. However, the Froude number must be higher than a critical Froude number F_D^C if the steady overturning bow wave expected to be generated when the waterline entrance angle is larger than the critical value F_D^C. F_D^C can be expressed as

$$F_D^C(\alpha_E) = \frac{4.4tan\alpha_E}{cos\alpha_E} - 1 \quad (6)$$

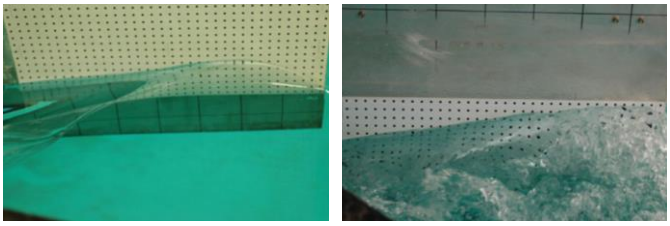

Fig. 3 Examples of two main bow waves genereated by a rectangular flat plate towed at the incidence α_E and flare angle γ in a tank. The two photographs are from Noblessse et al. (2008).

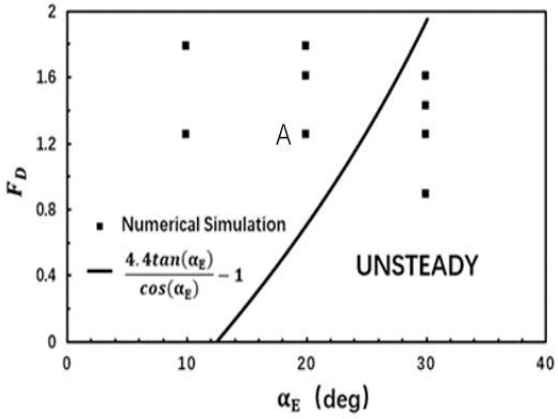

Fig. 4 The theoretical boundary defined by $\frac{4.4tan\alpha_E}{cos\alpha_E} - 1$ is corresponding to the solid line. The cases that are simulated are marked on this figure with ■. The point A corresponds with case 6 (α_E=20°, γ=15° F_D=1.6063).

The boundary between the steady wave and the unsteady wave defined by the Eq. 6 is shown in Fig. 4. One point identified as points A which is corresponding to case 6 is depicted in the figure. Point A is located inside the steady-flow region. The flow state of the point A is the steady overturning bow wave which is consistent with the theoretical result. The snapshots of the time sequence of overturning bow wave (point A) are presented in Fig. 5. The process shown in the Fig. 5 is divided into three parts. The wave crest becomes steep and reaches its maximum height. The overturning bow wave forms due to the overturning jet shooting out from the wave face, which is shown in Fig. 5(a). The overturning wave hits the free surface in Fig. 5(b). Fig. 5(c) shows the second impact occurs owing to striking the free-surface.

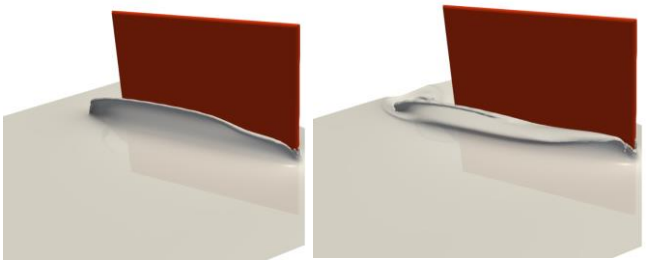

(a) Formation of the overturning bow wave

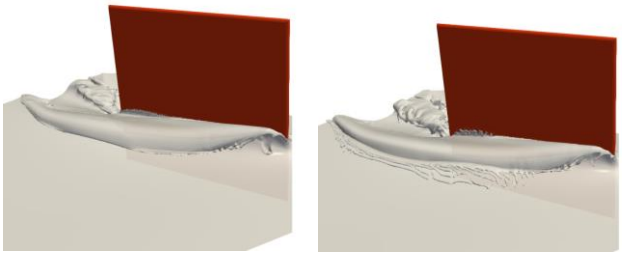

(b) Striking the free-surface

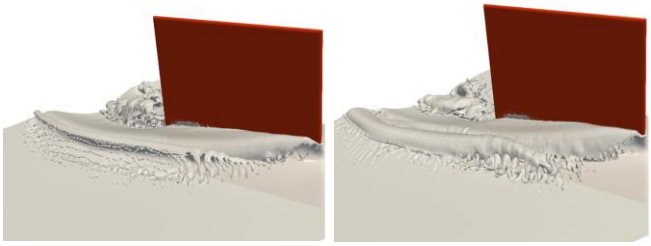

(c) Occurrence of the second impact

Fig. 5 The process of a steady overturning bow wave corresponding to point A.

The height of ship bow wave

As mentioned above, a simple approximation of the height of ship bow wave is given by Noblesses et al. (2006). The expression can be given as:

$$Z_b = C^Z \frac{\tan \alpha_E}{\cos \alpha_E} \frac{U^2/g}{1+U/\sqrt{gD}} \tag{7}$$

where α_E and U represent the half-angel of waterline entrance and the speed of flow. D is draft. g indicates the gravitational acceleration. $C^Z \approx 2.2$ is a constant which is determined from available experimental measurements.

Eq. 7 expresses that the bow-height Z_b can be obtained explicitly if we know the ship draft, the waterline entrance angle $2\alpha_E$ and the ship speed U. In this paper, theoretical results of the bow-height Z_b of the cases in numerical simulation can be obtained according to the Eq. 7. The results of numerical simulations are compared to the theoretical results and the results of experimental measurements that are given by Noblessse et al. (2008) in order to verify the results of numerical simulations. The scaled height of the bow wave $\left(\frac{Z_b g}{U^2}\right) cos\alpha_E/tan\alpha_E$ which is computed with theoretical results and the results of the numerical simulations as a function of $F_D/(1+F_D)$ is depicted in Fig. 6. The result of numerical simulation agrees with the theoretical result and the result of experimental measurement.

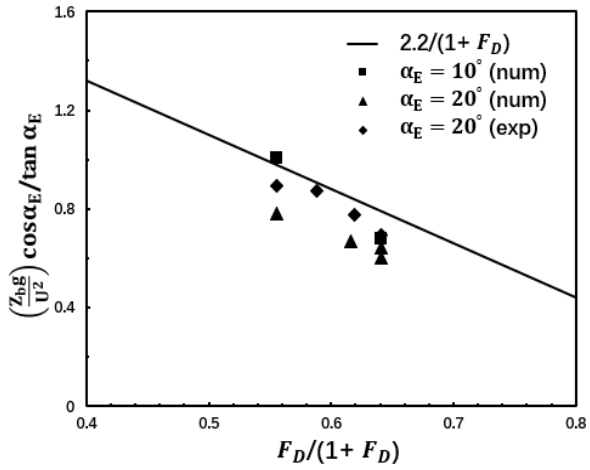

Fig. 6 The normalized height of $\left(\frac{Z_b g}{U^2}\right) cos\alpha_E/tan\alpha_E$ for theoretical results(solid line corresponding to $2.2/(1+F_D)$), numerical results($\alpha_E = 10^\circ, 20^\circ$, ■ , ▲) and the results of experimental measurements($\alpha_E = 10^\circ$,◆).

The distance between the crest of ship bow wave and ship stem

The location of the bow wave is also very important for ship design. We considered the distance between the ship stem and the crest of ship bow wave. A simple analytical expression for the distance was proposed by Noblesses et al. (2006) based on dimension analysis, thin-ship theory, shallow-draft and deep-draft limits. The expression can be given as:

$$X_b = \frac{C^X U^2/g}{1+U/\sqrt{gD}} \tag{8}$$

where U represents the speed of flow. D is draft. g indicates the gravitational acceleration. $C^Z \approx 1.1$ is a constant which is determined from available experimental measurements.

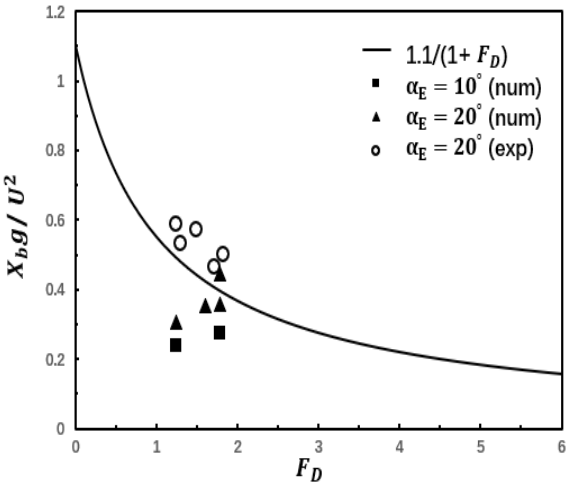

Fig. 7 The normalized distance of $\left(\frac{X_b g}{U^2}\right)$ for theoretical results(solid line corresponding to $1.1/(1+F_D)$) , numerical results($\alpha_E = 10^\circ, 20^\circ$, ■, ▲) and the results of experimental measurements($\alpha_E = 10^\circ$,○).

The Eq. 8 indicates that the distance between the crest of ship bow wave and ship stem only depends on the speed U and draft D. Similar to verification of the bow wave height. According to Eq. 8, theoretical results of X_b are obtained. The Fig. 7 depicts the normalized distance $X_b g/U^2$ as a function of the Froude F_D. The numerical results, theoretical results and experimental measurements which is given by Noblesses et al. (2008) are depicted in the Fig. 7 so the normalized distance of numerical simulation can be compared to the normalized distance of the approximation and experimental measurements. From figure, we find most of numerical results are well fit to theoretical results. Overall, the error of X_b is larger than the error of Z_b.

The solution of the constant C^Z and C^X with the results of numerical simulation.

The important step is to determine the constant C^Z and C^X when the Eqs. 7~8 are used. According to the approximation, we yield the Eqs. 9~10 to predict the constant. $C^Z = 2.2$ and C^X =1.1 are come from Ogilvie measurement of bow-wave height and location.

$$C^z = \frac{Z_b g}{U^2}\frac{cos\alpha_E}{tan\alpha_E}(1+F_D) \tag{9}$$

$$C^X = \frac{X_b g}{U^2 F_D} \tag{10}$$

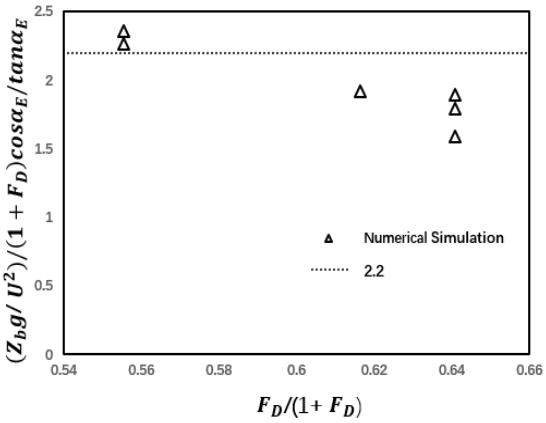

Fig. 8 The normalized $\frac{Z_b g}{U^2}(1+F_D)\frac{cos\alpha_E}{tan\alpha_E}$ as a function of $F_D/(1+F_D)$. The constant C^Z of the simple approximation of the ship bow wave for numerical simulation is marked with △. Dotted line is 2.2 which comes from experiment.

The constants are solved according to the Eqs. 9~10. The normalized parameters $\frac{Z_b g}{U^2}(1+F_D)\frac{cos\alpha_E}{tan\alpha_E}$ and $(X_b g/U^2)/F_D$ as a function of $F_D/(1+F_D)$ are depicted in Fig. 8 and Fig. 9. The values that are from experimental measurements are also depicted in Fig. 8 and Fig. 9. From the figures, we find the constant from numerical simulation are up and down around the results that are from experimental measurements. The result of numerical simulation is consistent with experimental measurements within a certain of error

Details analysis of overturning bow wave

The overturning bow wave process has been presented in Fig. 5. More details of the overturning bow wave process are shown here. In order to capture more details, the ship bow region is refined. The first impact and second impact can be observed when overturning bow waves hit the main body of water, which is in agreement with experiment observations. A pocket of air is entrapped when overturning jet is projected forwards from the crest of the wave. Some small-scale structures such as jets are also found in Fig. 10.

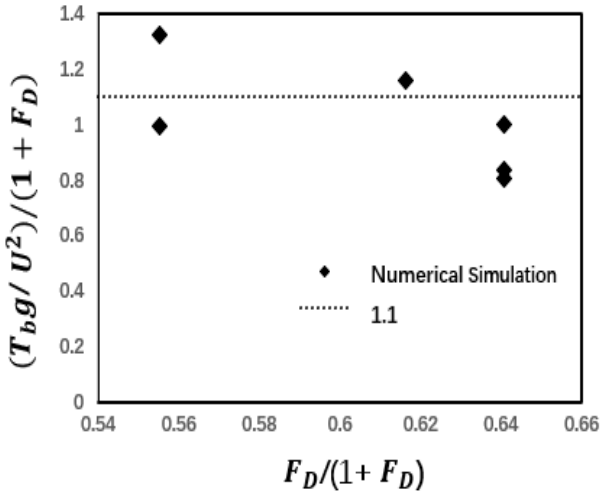

Fig. 9 The normalized $(X_b g/U^2)/F_D$ as a function of $F_D/(1+F_D)$. The constant C^X of the simple approximation of the ship bow wave for numerical simulation is marked with ◆. Dotted line is 1.1 which comes from experiment.

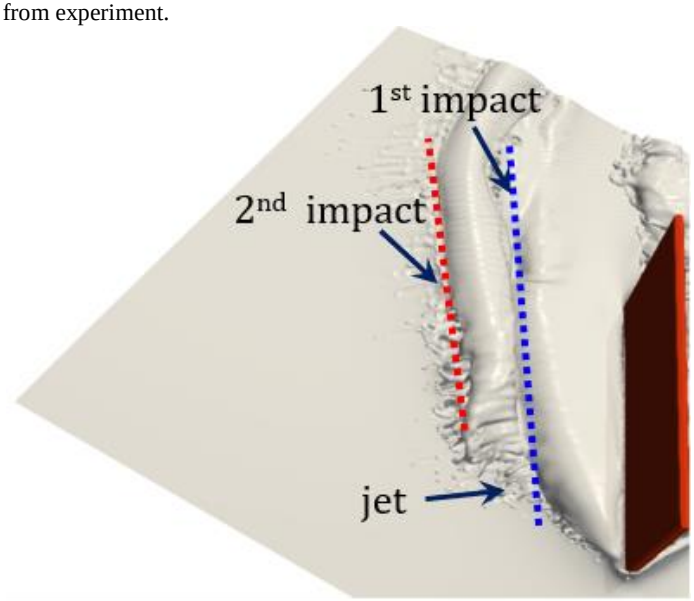

Fig. 10 Typical overturning bow wave

CONCLUSIONS

In this paper, the bow waves generated by a towed rectangular plate were simulated. Ten different cases with various incidence angle α_E, Flare angle γ and draft Froude number F_D were performed. We focus on the height and location of the bow wave which are very important for ship design at early stage. The results of numerical simulation are in agreement with theorical results and experiment measurements. The constant C^Z and C^X in the expressions which are determined with the results of numerical simulation are consistent with the experimental measurement. The refinement of ship bow region is shown and more details (the first impact, the second impact and the jet) are found. In general, the numerical simulations are in agreement with the simple approximation and experimental measurements.

ACKNOWLEDGEMENTS

This work is supported by the National Natural Science Foundation of China (11902199, 51979160, 51879159), Shanghai Pujiang Talent Program (19PJ1406100), The National Key Research and Development Program of China (2019YFB1704200, 2019YFC0312400), Chang Jiang Scholars Program (T2014099), Shanghai Excellent Academic Leaders Program (17XD1402300), and Innovative Special Project of Numerical Tank of Ministry of Industry and Information Technology of China (2016-23/09), to which the authors are most grateful.

REFERENCES

Chen, G, Kharif, C, Zaleski, S, and Li, J (1999). "Two-dimensional Navier–Stokes simulation of breaking waves," *Physics of Fluids*, 11(1), 121-133.

Delhommeau, G, Guilbaud, M, David, L, Yang, C, and Noblesse, F (2009). "Boundary between unsteady and overturning ship bow wave regimes," *Journal of Fluid Mechanics*, 2009, 620, 167-175.

Dommermuth, DG, Sussman, M, Beck, RF, Oshea, TT, Wyatt, DC, Olson, K, and Macneice, P (2004). "The Numerical Simulation of Ship Waves Using Cartesian Grid Methods with Adaptive Mesh Refinement," *25th Symposium on Naval Hydrodynamics*, Canada, 1-13.

Dong, RR, Katz, J, and Huang, TT (1997). "On the structure of bow waves on a ship model," *Journal of Fluid Mechanics*, 346, 77-115.

Kim, S and Lee, Y (2001). "Numerical Simulation of Breaking Waves around a Two-Dimensional Rectangular Cylinder Piercing Free Surface," *Journal of ship and ocean technology*, 5(4), 29-43.

Liu, C, and Hu, CH (2014). "An efficient immersed boundary treatment for complex moving object," *Journal of Computational Physics*, 274, 654-680.

Liu, C, and Hu, CH (2018). "Block-based adaptive mesh refinement for fluid structure interactions in incompressible flows," *Computer Physics Communications*, 232, 104-123.

Lubin, P, and Glockner, S (2015). "Numerical simulations of three-dimensional plunging breaking waves: generation and evolution of aerated vortex filaments," *Journal of Fluid Mechanics*, 2015, 767, 364-393.

Noblesse, F, Hendrix, D, Faul, L, and Slutsky, J (2006). "Simple Analytical Expressions for the Height, Location, and Steepness of a Ship Bow Wave," *Journal of Ship Research*, 50(4), 360-370.

Noblesse, F, Delhommeau, G, Guilbaud, M, Hendrix, D, and Yang, C (2008). "Simple analytical relations for ship bow waves," *Journal of Fluid Mechanics*, 600, 105-132.

Ogilvie, TF (1972). "The wave generated by a fine ship bow,"*9th International Symposium on Naval Hydrodynamics*, Paris, 1483–1524.

Olivieri, A, Pistani, F, Wilson, R, Campana, EF, and Stern, F (2007). "Scars and Vortices Induced by Ship Bow and Shoulder Wave Breaking," *Journal of Fluids Engineering*, 129(11), 1445-1459.

Shakeri, M, Tavakolinejad, M, Mayer, M, and Duncan, JH (2006). "Characteristics of Breaking Bow Waves Generated by a 2D+T Wave Maker," *Asme Joint Us-european Fluids Engineering Summer Meeting Collocated with International Conference on Nuclear Engineering*, Miami, 2, 85-90.

Waniewski, TA, Brennen, CE, and Raichlen, F (2001). "Measurements of Air Entrainment by Bow Waves," *Journal of Fluids Engineering*, 123(1), 57-63.

Wang, JH, and Wan, DC (2018). "CFD Investigations of Ship Maneuvering in Waves Using naoe-FOAM-SJTU Solver," *Journal of Marine Science and Application*, 2018, 17(3), 443-458.

Wang, JH, and Wan, DC (2020). "CFD Study of Ship Stopping Maneuver by Overset Grid Tec hnique," *Ocean Engineering*, 2020, 197, 106895.

Wang, JH, Ren, Z, and Wan, DC (2020). "Study of a Container Ship with Breaking Waves at High Froude Number Using URANS and DDES Methods," *Journal of Ship Research*, 2020.

Wang, JH, Zhao, WW, and Wan, DC (2019). "Simulations of Self-Propelled Fully Appended Ship Model at Different Speeds," *International Journal of Computational Methods*, 2019, 16(5), 1840015.

Wang, JH, Zhao, WW, and Wan, DC (2019). "Development of naoe-FOAM-SJTU solver based on OpenFOAM for marine hydrodynamics," *Journal of Hydrodynamics*, 2019, 31(1): 1-20.

Waniewski, TA, Brennen, CE, and Raichlen, F (2002). "Bow Wave Dynamics," *Journal of Ship Research*, 46(1), 1-15.

Wilson, RV, Carrica, PM, and Stern, F (2007). "Simulation of ship breaking bow waves and induced vortices and scars," *International Journal for Numerical Methods in Fluids*, 54(4), 419-451.